Kwon, M., & Han, D. (2019). Assessment of remotely sensed soil moisture products and their quality improvement: a case study in South Korea. *Journal of Hydro-environment Research*, *24*, 14-27. https://doi.org/10.1016/j.jher.2019.04.002

Assessment of remotely sensed soil moisture products and their quality improvement: a case study in South Korea

Moonhyuk Kwon[1]* and Dawei Han[1]

[1]Water and Environmental Management Research Centre, Department of Civil Engineering, University of Bristol, Bristol, UK

*Corresponding author: Moonhyuk Kwon (mk15217@bristol.ac.uk)

[1] Civil and Environmental Engineering, University of Bristol, United Kingdom

Abstract

Soil moisture (SM) retrieved from satellite observations has become available at a global scale with relatively high spatial-temporal resolution, and the satellite-derived SM can be useful data sources where in-situ measurements are scarce or not available. In this study, the SM data from two different satellite sensors, the Advanced Scatterometer (ASCAT) and Advanced Microwave Scanning Radiometer 2 (AMSR2), are evaluated through the comparison with in-situ observation collected from twelve sites over a three-year period (2013-2015) in South Korea. The results reveal that the ASCAT descending overpass (09:30, the local equatorial crossing time) shows a better correlation with the in-situ observation than the ascending overpass (21:30, the local equatorial crossing time), while no significant difference in performance is found for AMSR2. Moreover, ASCAT SM retrieval shows a generally better agreement with in-situ observation. Considering the spatial mismatch and different measurement depths, a cumulative distribution function (CDF) matching method, as well as an exponential filter method, are employed to improve the applicability of satellite-derived SM. Specifically, the observation operators based on CDF matching are derived to find the optimal temporal period and tested by cross-validation. It is found that the CDF matching method split into two groups (i.e., growing and non-growing season) outperforms the other temporal groups. Additionally, considering different observation depths between the in-situ (> 10 cm) and the satellite products (the top soil layer), the root-zone SM (RZSM) is derived from satellite surface SM by using the exponential filter method. For this study, a characteristic time length (T) at each observation depth is optimized by maximizing the *r* value between the SWI and the in-situ observation. Although the optimal T value generally increases with observation depth, it is clearly seen that T values are highly location-dependent. Given an encouraging improvement of the satellite SM estimation when scaling and filtering method applied, the results obtained in this study show that the satellite SM products have the useful potential for operational applications.

Keywords: ASCAT; AMSR2; Soil moisture; Remote sensing; Cumulative distribution matching

1. Introduction

Soil moisture (SM) plays a fundamental role in understanding land-atmosphere interactions although it comprises less than 0.001% of the total global water budget (Barrett and Petropoulos, 2013). SM information is therefore an essential hydrological variable and a key parameter to quantify and monitor water-related processes such as weather prediction, runoff forecasting, crop-yielding monitoring, and flood risk assessment (Scipal et al., 2008; Brocca et al., 2011; Paulik et al., 2014). In this respect, acquiring continuous and accurate information of spatiotemporal SM is of great importance in hydrology, meteorology and agriculture (González-Zamora et al., 2016).

SM estimates can be obtained from ground-based measurement, satellite observation and SM accounting model, as well as an integration of different sources of data to address each method's limitation. In-situ observation is generally recognized as a tool for gaining accurate SM information, and therefore commonly used as a reference variable for hydrological applications (Dorigo et al., 2011). Yet, gathering such data remains challenging for many parts of the world with respect to their spatiotemporal aspects (Brocca et al., 2017; Peng et al., 2017; Zhuo and Han, 2016), which, in turn, has contributed to the popularity of using SM products from space. Another practical issue is that hydrological analysis is typically implemented on a catchment scale, while point-based measurements tend to be poorly representative of the spatial distribution for a large-scale estimation of SM due to heterogeneous land surface (Griesfeller et al., 2016; Reichle et al., 2004; Wagner et al., 2013).

Considering these limitations, remotely sensed SM has become an important complementary tool for monitoring SM conditions, providing the advantage of relatively large-scale and high temporal coverage (Brocca et al., 2011; Zeng et al., 2015). The reliability of SM estimates from microwave sensors, both active and passive, has been investigated in depth since their launch. Compared with other remote sensing techniques that use visible and infrared radiation, microwave remote sensing techniques using longer wavelengths have the potential to offer SM products in that they are mostly unaffected by weather conditions such as cloud cover, haze, rainfall, and aerosols (Barrett and Petropoulos, 2013; Chauhan et al., 2003). Currently, several space missions employing microwave remote sensing have been in operation, providing surface SM measurements in near real-time (Brocca et al., 2017). The European Space Agency's (ESA) SMOS mission, operating since November 2009, is the first satellite dedicated to measuring surface SM and ocean salinity (Kerr et al., 2012). SMOS detects the brightness temperature at the frequency of 1.4 GHz (L-band, 21 cm), which is able to penetrate up to approximately 5 cm of soil (Ford et al., 2014). NASA's Soil Moisture Active and Passive (SMAP) mission was launched in January 2015 into the sun-synchronous 6 am/6 pm orbit with an objective to produce a global mapping of high-resolution SM every 2-3 days using an L-band (active) radar and L-band (passive) radiometer (Entekhabi et al., 2010). We attempted to evaluate SMOS and SMAP soil moisture products. However, the number of available data acquired from both satellites was too small for their effective evaluation. It is widely accepted that observations at L-band are severely perturbed by Radio Frequency Interference and (RFI) (Colliander et al., 2017), and Asia and Europe together comprise the majority of RFI sources in the world (Oliva et al., 2012). In this respect, Zeng et al. (2015) have suggested that in Asia, known as the most contaminated area by RFI, it is better to use other satellite sensors instead of the SMOS.

There are also two other sensors that have been widely used for SM retrieval from remote sensing: ASCAT on board the Meteorological Operational (METOP) satellite (Albergel et al., 2008b) and AMSR2 on board the Global Change Observation Mission (GCOM)-W1 satellite (JAXA, 2013). Based on practical considerations (i.e., data availability) as well as the results of the previous studies, this study is dedicated to evaluating satellite soil moisture products from ASCAT and AMSR2 and improving their quality for the practical issue. In the past few decades, many studies have been conducted to examine the accuracy of active and passive microwave sensors and to expand their applicability for practical issues in hydrology. For example, Wu et al. (2016) evaluated AMSR2 by analyzing ascending and descending overpass products to each other as well as comparing 598 in-situ SM observation stations from the International Soil Moisture Network. Their findings reveal that AMSR2 SM retrievals tend to underestimate in-situ measurements, and similar results were obtained by Zeng et al. (2015) over the Tibetan Plateau region. In contrast to AMSR2, which uses passive microwave sensing techniques, ASCAT provides a global satellite-based active microwave SM product. Validation studies based on ASCAT have been mainly carried out across Europe, and the results show that ASCAT could produce SM with a reasonable level of accuracy (Albergel et al., 2008a; Brocca et al., 2010; Wagner et al., 2013; among others). Despite the potential advantages of satellite-based remote sensing techniques, one of the primary issues is that they are only able to monitor a very thin soil layer, while the RZSM provides more meaningful information in some cases for hydrological applications, such as drought monitoring and crop-yielding prediction (Ford et al., 2014). The limitations associated with their observation depth have led to introducing new approaches to derive the RZSM from the surface SM. For instance, data assimilation techniques, such as Extended Kalman Filter and Ensemble Kalman Filters, have been proposed to combine satellite surface SM with a different source of data to reproduce the RZSM (Renzullo et al., 2014; Sabater et al., 2007). Additionally, Zaman and Mckee (2014) used a machine learning scheme to predict the RZSM by assimilating surface SM, soil temperature and precipitation datasets. However, the above-mentioned schemes have a high computational cost (González-Zamora et al., 2016). Alternatively, the exponential filter method used in this study, also known as Soil Water Index (SWI), proposed by Wagner et al. (1999), has been widely used owing to its relative simplicity and applicability (Albergel et al., 2008a, 2008b; Ceballos et al., 2005; Ford et al., 2014; Paulik et al., 2014; Qiu et al., 2014).

In addition to the filtering method, scaling techniques are frequently adopted to minimize systematic differences between remote sensing-derived and site-specific SM (Brocca et al., 2011; Su et al., 2013; Kornelsen and Coulibaly, 2015). The scaling methods include the cumulative distribution function (CDF) matching method (Cenci et al., 2016; Enenkel et al., 2016; Massari et al., 2015; Paulik et al., 2014), linear regression, linear rescaling, and Min/Max correction. Most of the conventional CDF matching schemes are carried out based on predefined temporal scales (i.e., monthly or seasonal bases). Monthly precipitation datasets were used to match the CDFs between modelled climate data and in-situ observations with respect to a gamma transform (Lopez et al., 2009). Taking seasonal dependencies into account, Yang et al. (2010) optimized CDF matching by dividing daily precipitation into four groups (i.e., a season).

Unlike the above-mentioned studies, Kim et al. (2016) explored optimal time steps for CDF matching using daily precipitation. They found that 8-day period for a bias correction showed the best. Several studies on the CDF matching method have been explored to derive observation operators, with the intention of building a statistical relationship with reference datasets. For instance, Gao et al. (2013) used observation operators derived from the CDF matching method to estimate the spatially averaged SM from point measurements. Similarly, the spatial transferability of observation operators was confirmed by Han et al. (2012). They found that the derived observation operators were successfully tested in space. Yet, the observation operators obtained from CDF matching approaches have rarely been assessed to the different combination of temporal groups.

Given this background, this study aims to address the following questions:

(1) What is the reliability of the SM retrievals from satellite sensors (ASCAT and AMSR2) and how do their performances in South Korea differ from the other parts of the world? Does the acquisition time (i.e., ascending and descending overpass) affect the quality of satellite SM retrievals?

(2) How could the applicability of satellite SM be improved? Is it desirable to apply the SWI approach for deriving RZSM from the surface, and are there any limitations to using the SWI method?

(3) Is the CDF matching method a useful post-processing scheme for mitigating the systematic biases between in-situ and satellite data? Do the different combinations of temporal periods affect the results?

We here first explore the accuracy of the original satellite SM retrievals in terms of their orbits as well as temporal variation patterns. Then, the SWI, combined with the CDF matching method, is suggested for the performance of the original satellite SM retrievals to be improved so as to be applicable to practical issues. Specifically, the selection of the optimal characteristic time (T) based on the SWI is carefully examined, and its dominant features are further identified. Additionally, besides the conventional CDF matching method that uses the whole record of the investigation period, we explore the performance of CDF matching method on a different temporal resolution basis to select an ideal combination: monthly (12 groups), seasonal (4 groups) and growing and non-growing (2 groups). The performance of each bias-correction group is then validated through a cross-validation procedure. Although the case study site is in South Korea, the methodology and results of this research are useful and relevant to the wider hydrological community.

2. Study area and soil moisture measurement

2. 1. Study area

The Korean peninsula, located in northeast Asia, has a range of 33°-38°N latitude and 124°-131°E longitude. Figure 1 shows the study areas along with twelve in-situ SM observation stations throughout South Korea.

[Insert Figure 1]

South Korea's climate is characterized by a cold, relatively dry winter and a hot, humid summer. In terms of rainfall, two-thirds of the annual rainfall (1,277 mm) comes during the flood season (between June and September) and only one-fifth of the rainfall comes during the dry season (from November to April of the following year), leading to challenging conditions for effective water resources management.

[Insert Table 1]

2.2. Soil moisture measurements

2.2.1. In-situ soil moisture measurements

The observed SM data collected in this study are managed by two organizations: 1) Korea Meteorological Administration (KMA) and 2) Korea Water Resources Cooperation (K-water). The SM contents at depths of 10, 20, 40 and 50 cm have been measured by KMA, while K-water has provided SM observations at different measurement depths (10, 20, 40, 60, 80 cm). A total of 12 sites across South Korea are selected in this study. SM data collected from KMA are measured by using Frequency Domain Reflectometry (FDR) sensors providing volumetric SM, while K-water provides SM data in the Yongdam Dam (YD) catchment by using Time Domain Reflectometer (TDR). The main characteristics of each observation site can be seen in Table 1. Here, the in-situ observations corresponding to satellite overpass time are used for the subsequent study. These observation datasets are assumed as the ground truth in assessing the satellite SM products.

2.2.2. Satellite soil moisture measurements

The Advanced Scatterometer (ASCAT) on board the METOP satellite crossing the Equator at the local times of 09:30 (descending orbit) and 21:30 (ascending orbit) was initially designed to monitor wind speed and direction over the ocean using an active microwave remote sensing (Wagner et al., 2013). The ASCAT is a C-band radar operating at 5.3 GHz, and its SM retrieval algorithm was developed by the Vienna University of Technology (TU Wien). Apart from its initial purpose, the results of numerous validation studies carried out around the world have yielded clear evidence that the ASCAT also provides SM estimates with high reliability (Wagner et al., 2013). In addition, the ASCAT produces SM products with reasonable temporal resolution (at a sampling time step of 1-3 days) and spatial resolution of 25-50 km (Figa-Saldaña et al., 2002). The ASCAT SM products can be obtained from either the European Organisation for the Exploitation of Meteorological Satellites (EUMETSAT) or the H-SAF Products Download Centre (http://hsaf.meteoam.it). In this study, the ASCAT SM time series products (H109 Metop ASCAT DR2016) with a 12.5-km spatial resolution (resampled from a 25-km grid), which represents the water content in the upper soil layer in relative units between 0% (driest condition) and 100% (wettest condition), were collected from H-SAF (accessed on 28 July 2016). Details on the conditions for access and use can be found on the distributor's web page.

AMSR2 is the Advanced Microwave Scanning Radiometer 2 on board the GCOM-W1 satellite, which was launched by the Japan Aerospace Exploration Agency (JAXA) in May 2012. Unlike the ASCAT, which uses active microwave remote sensing techniques, the AMSR2 is a passive microwave sensor, taking measurements at multiple frequencies to provide various hydrological parameters. The AMSR2 was developed to measure the brightness temperatures at seven different frequencies including 6.925/7.3 GHz, 10.65 GHz, 18.7 GHz, 23.8 GHz, 36.5 GHz, and 89.0 GHz and was initially designed to observe various parameters connected to the hydrological cycle, such as precipitation, wind speed, snow depth, SM content, and others (Imaoka et al., 2010).

As a successor to AMSR-E, which was in operation from May 2002 to October 2011, the basic concept of AMSR2 is almost the same as that of AMSR-E. However, AMSR2 shows improvements compared with its predecessor; a 7.3-GHz channel was added to identify and address Radio Frequency Interference (RFI) signals, and AMSR2's antenna diameter was enlarged to 2 meters (AMSR-E's measures 1.6 meters) for better spatial resolution (JAXA, 2013; Wu et al., 2016). AMSR2 SM products, which are derived from two different algorithms either the JAXA (Koike, 2013) or Land Parameter Retrieval Method (LPRM; Owe et al., 2008) algorithm can be obtained from each distributor's website (https://gcom-w1.jaxa.jp for JAXA and http://gcmd.gsfc.nasa.gov for LPRM). Unlike the JAXA algorithm, which uses a 10.7 GHz channel, the LPRM product provides AMSR2 SM retrievals for the 6.9 (C-band), 7.3 (C-band) and 10.7 GHz (X-band). Before utilizing the AMSR2 SM product, each dataset (one dataset from the JAXA algorithm accessed on 4 April 2016 and three datasets from the LPRM algorithm accessed on 25 January 2017) was compared to the in-situ observation for evaluation. Based on our preliminary analysis, the JAXA algorithm showed the best agreement with in-situ observation in terms of the correlation coefficient. The results are discussed more in detail in section 4. JAXA AMSR2 Level 3 (hereinafter AMSR2) SM products (with 0.1° spatial resolution and volumetric terms (%)) were selected for further analysis in this study.

3. Methodology

The satellite SM product sets retrieved from both ASCAT (active microwave sensor) and AMSR2 (passive microwave sensor) are compared with the in-situ SM observations (as ground truth) to evaluate their performance. The satellite pixel values whose centroids are located nearest to each ground observation site are extracted from both satellites. Owing to differences in spatial-temporal resolutions as well as observation depths between satellite and point measurements, satellite data are usually scaled and/or filtered before their utilization for actual applications (Scipal et al., 2008). In the first step, given that SM estimates are provided by different units (volumetric terms for both in-situ and AMSR2, and relative SM for ASCAT), we normalized all the data by using the maximum and the minimum values over the investigation period through the following equation:

$$Z_i = \frac{x_i - min(x)}{max(x) - min(x)} \tag{1}$$

where Z_i is the normalised SM time series, and $max(x)$ and $min(x)$ are the maximum and minimum value of the investigation period, respectively. After employing the normalising method, both satellite data and in-situ observations have the same maximum and minimum values.

3.1. Filtering technique

Satellite-retrieved SM is representative of a topsoil layer (i.e., satellite-based SM estimates have inherent limitations in capturing the variation of the RZSM), while the RZSM is more readily applicable to be incorporated into hydro-meteorological models (Brocca et al., 2012; Dharssi et al., 2011). In this sense, one popular semi-empirical approach, the exponential filter technique also known as Soil Water Index (SWI) proposed by Wagner et al. (1999), is employed to derive the RZSM from near-surface observations. In spite of the potential lacks of a physical interpretation (Manfreda et al., 2014), many studies have extensively used this scheme, owing to its simplicity of implementation, computational efficiency and robustness for representing the RMSE. This scheme assumes that a soil profile consists of the surface layer and subsurface layer, and the SM dynamics of the lower layer is proportionally linked with the difference between the two layers. A recursive formulation of the exponential filter that is relatively easy to implement but provides a mathematically equivalent principle to the original filter method is adopted in this study following Albergel et al. (2008b):

$$SWI_n = SWI_{n-1} + K_n\,[SSM_{(t_n)} - SWI_{n-1}] \tag{2}$$

where SWI_n is the estimated profile SM at t_n. Eq. (4) is initialized with $SWI_0 = SSM_{(t_0)}$ and $K_0 = 1$, respectively. $SSM_{(t_n)}$ refers to the surface SM estimate at t_n, and the gain K at time t_n is given by:

$$K_n = \frac{K_{n-1}}{K_{n-1} + e^{-\frac{(t_n - t_{n-1})}{T}}} \tag{3}$$

where T is a surrogate parameter (generally named characteristic time length) that characterizes the temporal dynamics of SM along the soil profile. t_n and t_{n-1} are the observation times of the current and the previous SSM measurement in Julian days. In this study, the T value is determined by optimizing the correlation coefficient (*r*) between SWI and in-situ observation. In other words, the T value corresponding to the highest correlation between the SWI and in-situ observation is considered as the optimal characteristic time length (T) for each SM observation stations.

The derived SWI is then compared with in-situ SM with respect to different observation depths along with SM profile (θ_{0-60}). In this study, the profile SM referring to depthweighted mean SM content between the land surface and a 60cm soil depth is computed as follows:

$$\theta_{0-60} = \frac{\theta_i \cdot d_i + \frac{\theta_i + \theta_{i+1}}{2}(d_{i+1} - d_i) + \frac{\theta_{i+1} + \theta_{i+2}}{2}(d_{i+2} - d_{i+1}) + \frac{\theta_{i+2} + \theta_{i+3}}{2}(d_{i+3} - d_{i+2})}{d_{i+3}} \tag{4}$$

where d_i(cm) represents the *i*-th depth of measurement from the top layer, and θ_i(%) is the SM obtained from the *i*-th depth. In the case where measurements at the 60 cm depth are not available, the values at the 60 cm depth were replaced by SM measurements at the 50 cm depth. Considering hydrological applications such as runoff modelling, flood forecasting, and drought monitoring, the average SM greater than the top soil layer is of great importance (Brocca et al., 2011; Paulik et al., 2014). In this regard, we attempt to compare the derived SWI with each soil layer as well as the depth-averaged SM contents.

3.2. Scaling technique

The mismatch in spatial scale and measuring depth between satellite-based retrievals and in-situ observations are likely to cause inevitable systematic differences. The cumulative density function (CDF) matching approach is considered to be an enhanced nonlinear technique applied to tackle systematic differences between different data sources (Su et al., 2013; Brocca et al., 2011; Liu et al., 2011; Scipal et al., 2008). Through this method, the satellite data are rescaled in such way that its CDF is matched with that of the in-situ measurements. In other words, the satellite SM products are mapped to the same probability value as that of observations.

$$Z_j = F_{oj}^{-1}\left(F_{sj}\left(\hat{Y}_{\mathrm{j}}\right)\right) \tag{5}$$

where $\hat{Y}_{\mathrm{j}}$ is a biased data (satellite product), Z_j is the bias corrected data (CDF matched value), F_{sj} is a CDF of biased data, and F_{oj}^{-1} is an objective CDF.

Here, the CDF of the two datasets (i.e., the satellite-derived SWI and observations) is firstly displayed, and then the differences corresponding to the CDF of each ranked data are computed. The observation operator is finally derived based on a polynomial fit, which allows defining site-specific parameters. To be specific, the parameters of the polynomial equation are estimated from one subset, and the derived parameters are then exploited to the remaining data set for validation. In addition, we test the performance of observation operators based on four different temporal groups. More groups are likely to result in reducing error, while using too many groups can lead to the overfitting issue. To avoid overfitting, the parameters obtained the calibration period are tested for validation.

3.3 Performance Indices

The performance and accuracy of satellite SM products are assessed by comparing them against in-situ observations that are regarded as reference SM values. For this study, four commonly used statistical indicators (i.e., correlation coefficient (*r*), root mean square error (RMSE), unbiased RMSE (ubRMSE) and bias) are computed to quantify the level of accuracy (Zeng et al., 2015). Here, for *N* discrete datasets of two variables (i.e., satellite SM retrieval (θ_s) and in-situ observation (θ_n)), the Pearson correlation coefficient (*r*) is used to examine temporal pattern similarity between two datasets, given by:

$$r = \frac{\frac{1}{N}\sum_{n=1}^{N}(\theta_S - \overline{\theta_S})(\theta_n - \overline{\theta_n})}{\sigma_S\,\sigma_n} \tag{6}$$

where σ_S and σ_n represent the standard deviation of satellite and in-situ SM, respectively. The overbar indicates the averages over the entire investigation period. In addition to the correlation coefficient, root mean squared error (RMSE) and unbiased root mean squared error (ubRMSE) are used for the validation of satellite SM products. $RMSE$ and $ubRMSE$ are calculated as follows:

$$RMSE = \sqrt{\frac{1}{N}\sum_{n=1}^{N}(\theta_n - \theta_s)^2} \quad (7)$$

$$ubRMSE = \sqrt{\frac{1}{N}\sum_{n=1}^{N}[(\theta_s - \overline{\theta_s}) - (\theta_n - \overline{\theta_n})]^2} \quad (8)$$

$ubRMSE$ is used for removing the systematic differences (i.e., bias) between satellite retrievals and in-situ observations. $ubRMSE$ is related with $RMSE$ and can be expressed as follows:

$$ubRMSE^2 = RMSE^2 + bias^2 \quad (9)$$

4. Results and Discussion

In this section, we evaluate the accuracy and reliability of the satellite-based SM products. The satellite SM products retrieved from both ASCAT and AMSR2 are compared with the in-situ observations collected from 12 different sites, over a three-year period for KMA sites (2013-2015), and a two-year period for YD sites (2014-2015).

4.1. Overview of the satellite soil moisture

Prior to evaluating the satellite-based SM products, we first attempt to explore the performance of SM retrieval algorithms (for AMSR2). Here, we assess each retrieval algorithm by comparing it with in-situ data measured at a depth of 10 cm. As for the LPRM algorithms, there is no significant improvement in accuracy by applying different frequencies (X, C1 and C2 band), with mean *r* values ranging between 0.13 and 0.17 for 12 observation sites (Table 2). Regarding the retrieval algorithm, AMSR2-JAXA also shows a negligible improvement in the performance, but satellite SM data with a higher spatial-temporal resolution can be obtained by using JAXA algorithm (10 km for JAXA and 25 km for

LPRM). Taking this advantage into account, the AMSR2 SM data derived from JAXA algorithm are hereinafter used for further studies.

[Insert Table 2]

As for polar orbit satellites, SM products are provided at different acquisition times (i.e., ascending and descending overpasses). The night-time retrievals are generally expected to have higher accuracy than the daytime products since the geophysical conditions are more favorable during the night-time (Kim et al., 2015; Zeng et al., 2015). On the other hand, there is also a positive effect over the daytime in that the canopy is more transparent and drier during the daytime (Brocca et al., 2011). Here, the daytime refers to the ascending overpass for AMSR2 (1:30 pm) and descending overpass of ASCAT (9:30 am), and vice versa for the night-time. In this regard, the performance associated with their overpass time is examined. For this study, in-situ observations measured at 10 cm depth corresponding to the satellite overpass times are used to evaluate the performance with respect to orbit direction. As can be seen from Figure 2, the descending retrieval for ASCAT is shown to be superior to the ascending one, while no significant discrepancy can be found for AMSR2.

[Insert Figure 2]

The results for ASCAT are in accordance with findings by Griesfeller et al. (2016) who obtained mean *r* values for Norway equal to 0.72 for the descending orbit (daytime) and 0.68 for the ascending orbit (night-time). Interestingly, they also found descending retrievals (night-time) to be in better agreement with in-situ observations for AMSR-E. In contrast, Zeng et al. (2015) obtained a higher *r* value for the ascending orbit in China (0.788 for night-time and 0.885 for daytime). The abovementioned studies indicate that the accuracy of SM data with respect to satellite orbit is highly location-dependent: SM products from the satellite can be affected not only by the orbits but also by other factors such as soil texture, topography, land cover, and climate. For instance, the *r* values for the KMA01 site are equal to 0.64 for the ascending overpass, 0.75 for the descending overpass, and 0.69 for the ascending plus descending overpasses (Figure 3). Compared to the descending overpass, the combination of ascending and descending overpasses shows a negligible decrease in performance in terms of *r* value. Furthermore, the combination of ascending and descending overpasses increases the temporal data coverage to 91% (N: 991) of date for the study period without any interpolation (Figure 3c). In this study, both of the ascending and descending products are used to obtain higher temporal coverage, which may help to provide more robust results by increasing the amount of data analyzed. For this reason, both passes were commonly used in many previous studies (Brocca et al., 2011; Kolassa et al., 2016)

[Insert Figure 3]

To examine how SM products perform seasonally and annually, a time series comparison of the different data sources from two sites is presented in Figure 4. The seasonal variation is strong over the study sites, displaying the characteristic of monsoons. The ASCAT products tend to overestimate in-situ data, while AMSR 2 generally underestimates the SM. The results are consistent with previous studies (Cho et al., 2015; Kim et al., 2015; Zeng et al., 2015). They also found that the AMSR 2 retrievals tend to underestimate in-situ SM with unrealistically high values responding to precipitation events and the lack of temporal dynamics.

[Insert Figure 4]

4.2. ASCAT versus in-situ observation

4.2.1. The exponential filter method

The microwave-based ASCAT products are representative of a very shallow soil layer (Brocca et al., 2011), whereas they are compared with in-situ observations measured greater than a depth of 10 cm. Moreover, the RZSM is a more important variable for many hydrological applications. In this regard, a recursive exponential filter method that allows estimating the RZSM from the surface measurement is employed. Then, the derived SWI from ASCAT surface SM products are compared with the in-situ SM observations at different depths along with the SM profile from surface to 50 cm depth ($\mathrm{d}_{0-50\ \mathrm{cm}}$). Here, correlation coefficient (*r*) is used for the selection of the optimal T, based on the fact that it is more meaningful to capture the temporal behavior of SM rather than the absolute value for many hydrological applications (González-Zamora et al., 2016). Table 3 shows the statistical performance between the ASCAT SWI and in-situ observations measured at different depths at 12 sites. The mean *r* values are 0.54, 0.52, 0.51, 0.47, and 0.58 at 10, 20, 30, 50, and 0-50 cm depth, respectively, and a slightly higher *r* value is obtained from the SM profile (0-50 cm).

[Insert Table 3]

In all the observation depths, the results show improved temporal correlations, indicating that the SWI method can reproduce the behavior of the RZSM. However, the relatively large differences in *r* values among the sites are found owing to systematic biases between the original satellite and in-situ observations. In terms of the mean RMSE, the figures are equal to 0.19, 0.21, 0.22, and 0.25 at the depths of 10, 20, 30 and 50 cm respectively, confirming a better performance of the SWI at the shallow soil layer. The differences in mean ubRMSE for each observation depth, however, are negligible ranging from 0.16 to 0.18. Considering relatively large differences between the ubRMSE and the RMSE (i.e., there remain systematic biases between in-situ and satellite SM dataset), it can be argued that bias reduction techniques should be employed to improve the accuracy of satellite retrievals with respect to in-situ observations.

The characteristic time length (*T*), representing the SM travel time from the surface, increases as the depth increases, which is in line with the assumption of the SWI (3.1 days for 10 cm and 8.3 days for 50 cm). The optimal T value for 0–50 cm shows similar results to those obtained for 10 cm, which shows that the SM stored in the top soil layer have more influence on the SM profile (0-50 cm). For SM profile (0-50 cm), one of the leading factors impacting the satellite SM is the ratio of open water surface within the pixel: the KMA01 site with the smallest ratio of open water surface (1.5%) has the best *r* value of 0.83 but the KMA06 site with the greatest proportion (9.1%) shows the lowest *r* value of 0.53 (Table 3). However, in the case of YD sites, the ratio of open water surface (< 2.0%) is much smaller than that of KMA sites, and there is no significant difference in *r* value according to the ratio of open water surface. However, some of the observation sites show surprising results of T values being smaller for the deeper soil layer. For instance, the optimal T value at the YD03 site appears to be inconsistent with the model assumption (i.e., 3.7 days for 10 cm depth and 1.5 days for 60 cm depth, respectively). A feasible explanation is presented in Figure 5, showing an example of the dynamic range of the SWI with respect to T values. Here, it is clear that as the T value increases, the time series of the ASCAT SWI becomes smoother (Figure 5a). In other words, the lower dynamic range with a larger T value is generally expected to be representative of SM contents at a deeper soil layer rather than a top soil layer. Interestingly, in this specific case, in-situ SM time series at a depth of 60 cm shows rather larger temporal variability compared with that measured at 10 cm depth, with a coefficient of variation (CV) equal to 31.61 for 10 cm and 39.31 for 40 cm (Figure 5b). The results are against the basic concept of the exponential filter method that assumes the SM content integrated over the deeper layers, thus exhibiting less variations than in the topsoil layer (González-Zamora et al., 2016). However, at some of the in-situ observations in this study, SM contents at the lower layer tend to respond more rapidly to rainfall, which may be caused by many uncertain factors. This abnormal SM variation at the deeper soil layer might be attributed to a preferential flow, causing an uneven and often rapid movement of water in the soil (Paquette et al., 2016). It is beyond the scope of this study to investigate this phenomenon further. Nonetheless, it should be noted that although the SWI approach is unlikely to capture short-term fluctuations that may occur in the root-zone in a particular area, the SWI method is a useful tool to build temporal dynamic of the RZSM.

[Insert Figure 5]

4.2.2. The CDF matching method

The CDF matching method is widely used in many hydrological applications to remove the systematic biases between two data sets. Here, the CDFs of the derived SWI are matched with those of in-situ observations at each site. The CDF matching method, in this study, is used to derive an observation operator through the third-order polynomial fit that has also been used in previous studies (e.g., Drusch et al., 2005; Han et al., 2012). The aim of using an observation operator is to define a set of parameters that are suitable for further use. In this study, besides the conventional CDF matching method that uses the whole record of investigation period (QM1), we explore the performance of CDF matching method on a different temporal resolution basis: monthly (12 groups; QM2), seasonal (4 groups; QM3) and growing and non-growing (2 groups; QM4). To be specific, the CDF matching method is built and validated for four different temporal groups: 1) the entire period of investigation, 2) monthly, 3) seasonal (spring (Mar-May), summer (Jun-Aug), fall (Sep-Nov) and winter (Dec-Feb)), and 4) growing (Apr-Sep) and non-growing seasons.

The proposed CDF matching approach is first tested to select an optimal temporal resolution in terms of statistical scores. For the sake of brevity, the results obtained at 10 cm only are presented. Taylor diagram is displayed in Figure 6, illustrating the statistical metrics of the comparison between in-situ observations and satellite retrievals with respect to the aforementioned temporal groups. Compared to the result obtained from ASCAT SWI (Table 3), it is clear that the ASCAT SWI-CDFs present enhanced performance scores, with the exception of QM1. To be specific, QM1 shows a fairly low range of correlations with most values being less than 0.77 (mean r = 0.54). On the other hand, the mean *r* values increase from 0.54 (ASCAT SWI) to 0.78, 0.77 and 0.78 for QM2, QM3 and QM4 respectively. As for ubRMSE values, they also generally show improved results, though not as significant as *r* values.

[Insert Figure 6]

To further ensure the applicability of the observation operators, we partitioned the datasets into two subsets. The datasets of ASCAT SWI are initially grouped based on temporal resolution. Then, the established parameters of the polynomial equation for the calibration period are validated for the remaining datasets. The performance of observation operators in both calibration and validation periods is presented in Figure 7. The observation operators behave differently between calibration and validation periods depending on temporal resolutions. The observation operators, in general, perform better in calibration than in validation periods. In terms of the correlation coefficient, the observation operator derived using QM1 shows a clearly worse performance compared to other temporal groups. Although both QM2 and QM3 display almost equally robust performances in statistical scores for calibration periods, the results obtained from the validation period show that the highest mean *r* values are observed when the datasets are grouped on the basis of growing and non-growing seasons (QM4). The similar results are generally observed with respect to the RMSE and ubRMSE.

[Insert Figure 7]

4.3. AMSR2 versus in-situ observation

The AMSR2 SM products are evaluated against ground SM observations with the same procedure as ASCAT: the scaling and filtering methods are also applied to assess and improve their performance.

4.3.1. The exponential filter method

It should be noted that the AMSR2 remote sensor provides SM information of the top soil layer depending on local surface conditions. Therefore, it is a huge challenge to obtain RZSM directly by means of remote sensing technique. In this regard, we derive the AMSR2 SWI using the exponential filter and then the derived RZSM at each observation depth is compared with in-situ observations. Here, the first step is to obtain optimal *T* at each site by computing to maximize the correlation coefficient. Then, the derived SWI is compared with in-situ observations. Table 4 shows the statistical scores describing the agreements between the AMSR2 SWI and in-situ observations measured at different depths. The average *r* values are equal to 0.36, 0.33, 0.34, 0.39, and 0.38 at 10, 20, 30, 50, and 0-50 cm depth, respectively, and a slightly higher mean *r* value is obtained from SM profile (0-50 cm). The mean RMSE for each observation depth ranges from 0.36 to 0.43 and the mean ubRMSE is from 0.18 to 0.19. The performance scores for AMSR2 are fairly lower than those obtained by ASCAT SWI. This is attributed to the discrepancy in the correlation of original AMSR2 data. It is interesting to note that the characteristic time (*T*) of the exponential filter is longer than that of ASCAT, with the average value of 10.6 days for AMSR2, and 3.1 days for ASCAT at 10 cm. The results are in line with previous studies that the optimal T highly varies depending on the study area, soil condition, climatic condition, and even satellite sensors used (Albergel et al., 2008a)

[Insert Table 4]

4.3.2. The CDF matching method

The proposed CDF matching approach is applied not only for addressing inevitable systematic biases between two different data sources but also for selecting an optimal temporal resolution. First, we test the CDF matching method for the entire investigation period and the results obtained at 10 cm are presented in Figure 8. It is clear that the CDF matching method provides enhanced performance scores for most of the bias-correction groups with the exception of QM1. The mean *r* values increase from 0.36 (AMSR2 SWI at 10 cm) to 0.39, 0.70, 0.60 and 0.68 for QM1, QM2, QM3 and QM4, respectively. The results obtained from QM1 are very similar to those derived from ASCAT, showing that the performance is apparently lower than the other groups. The QM2 based on a monthly duration shows the best performance among others: the RMSE ranges from 0.11 to 0.18, with the average value of 0.15; the *r* value is in the range 0.52-0.80, with the average value of 0.70.

[Insert Figure 8]

Given that too many groups can cause serious overfitting issues, we subdivided datasets into two subsets and then validated the proposed CDF matching method through cross-validation. As can be seen in Figure 9, it is evident that QM1 shows the worst performance in both calibration and validation periods. As for QM2 and QM3, significant different statistical scores are found between the calibration and validation periods resulting from overfitting issues. In contrast, QM4 shows a robust performance over both calibration and validation periods, thus confirming that the derived observation operator based on growing and non-growing seasons performs the best. These results are in accordance with the ASCAT.

[Insert Figure 9]

Figure 10 shows the samples of time series comparison of the SWI-CDF with the in-situ observations. The SWI-CDF for ASCAT and AMSR2 is found to capture the temporal variation of in-situ SM with an enhanced level of accuracy in comparison with original satellite SM products.

[Insert Figure 10]

5. Conclusion

This study aims to assess active and passive microwave SM retrievals and further expand their applicability. We first estimated the accuracy of the original satellite SM retrievals in terms of their orbits as well as variation patterns. For the ASCAT products, the descending overpass was more highly correlated with in-situ observations than the ascending overpass in the study area. Conversely, a slightly better correlation was found in the ascending overpass for the AMSR2 although the differences are insignificant. Next, the exponential filter, eventually combined with the CDF matching method, was employed to derive the RZSM that appears to be more meaningful than the surface SM for hydrological applications. Specifically, the selection of the optimal characteristic time (T) based on the Pearson correlation coefficient was carefully examined, and its notable features were further investigated. It is concluded that the optimal T values generally increase with the depth of observed soil, which is in accordance with the model's underlying assumption that T represents water travel time along the soil profile. However, a smaller T value was obtained in the deeper soil layer at some observation sites, indicating that SM contents at the deeper layer tend to show rather larger temporal variability compared with that measured at the lower layer. Based on the results achieved in this study, it should be noted that although the determination of the optimal T value depends mainly on the soil depth, T value is also influenced by many uncertain factors, such as soil properties, length of data and climate conditions.

Apart from the conventional bias correction approach that uses the whole record of the investigation period, we evaluated the performance of CDF matching method on a different temporal resolution basis to select an ideal combination: monthly (12 groups), seasonal (4 groups) and growing and non-growing (2 groups). The performance of each bias-correction group was then validated through a cross-validation procedure for the purpose of addressing overfitting issues. A bias-correction period of QM4 (2 groups) performed well for both calibration and validation periods in South Korea. However, it should be noted that the results achieved in this study might be location-dependent so that one can obtain different optimal temporal resolutions for other locations. Nonetheless, given that little work on this topic has been carried out to explore the optimal bias-correction period in the literature, the methodology we proposed in this study will encourage future research in this field.

Overall, the underlying features and some limitations of satellite SM retrievals were investigated in depth. Furthermore, successful attempts were made to overcome the shortcomings of the original satellite products. Despite our primary contribution in this study, further work is required to address this study’s limitations, i.e., the low number of observation sites as well as relatively short-term observation periods. Specifically, as for the proposed CDF matching method in this study, more stable and comprehensive results are expected with a more extended period of records.

Acknowledgement

The first author gratefully acknowledges the financial support provided by K-water for carrying out his PhD study at the University of Bristol. The AMSR2 data for this study were supplied by the GCOM-W1 Data Providing service (https://gcom-w1.jaxa.jp), and the ASCAT data were obtained from the H-SAF Products Download Centre (http://hsaf.meteoam.it). We would like to thank both KMA and K-water for providing the ground SM data.

References

Albergel, C., Rüdiger, C., Carrer, D., Calvet, J.-C., Fritz, N., Naeimi, V., Bartalis, Z., Hasenauer, S., 2008a. An evaluation of ASCAT surface soil moisture products with in-situ observations in southwestern France. Hydrol. Earth Syst. Sci. Discuss. 5, 2221–2250. https://doi.org/10.5194/hessd-5-2221-2008

Albergel, C., Rüdiger, C., Pellarin, T., Calvet, J.-C., Fritz, N., Froissard, F., Suquia, D., Petitpa, a., Piguet, B., Martin, E., 2008b. From near-surface to root-zone soil moisture using an exponential filter: an assessment of the method based on in-situ observations and model simulations. Hydrol. Earth Syst. Sci. Discuss. 5, 1603–1640. https://doi.org/10.5194/hessd-5-1603-2008

Barrett, B., Petropoulos, G., 2013. Satellite Remote Sensing of Surface Soil Moisture. Remote Sens. Energy Fluxes Soil Moisture Content 85–120. https://doi.org/doi:10.1201/b15610-6

Brocca, L., Crow, W.T., Ciabatta, L., Massari, C., De Rosnay, P., Enenkel, M., Hahn, S., Amarnath, G., Camici, S., Tarpanelli, A., Wagner, W., 2017. A Review of the Applications of ASCAT Soil Moisture Products. IEEE J. Sel. Top. Appl. Earth Obs. Remote Sens. 10, 2285–2306. https://doi.org/10.1109/JSTARS.2017.2651140

Brocca, L., Hasenauer, S., Lacava, T., Melone, F., Moramarco, T., Wagner, W., Dorigo, W., Matgen, P., Martínez-Fernández, J., Llorens, P., Latron, J., Martin, C., Bittelli, M., 2011. Soil moisture estimation through ASCAT and AMSR-E sensors: An intercomparison and validation study across Europe. Remote Sens. Environ. 115, 3390–3408. https://doi.org/10.1016/j.rse.2011.08.003

Brocca, L., Melone, F., Moramarco, T., Wagner, W., Hasenauer, S., 2010. ASCAT soil wetness index validation through in situ and modeled soil moisture data in central Italy. Remote Sens. Environ. 114, 2745–2755. https://doi.org/10.1016/j.rse.2010.06.009

Brocca, L., Moramarco, T., Melone, F., Wagner, W., Hasenauer, S., Hahn, S., 2012. Assimilation of surface- and root-zone ASCAT soil moisture products into rainfall-runoff modeling. IEEE Trans. Geosci. Remote Sens. 50, 2542–2555. https://doi.org/10.1109/TGRS.2011.2177468

Ceballos, A., Scipal, K., Wagner, W., Martınez-Fernandez, J., 2005. Validation of ERS scatterometer-derived soil moisture data in the central part of the Duero Basin, Spain. Hydrol. Process. 19, 1549–1566. https://doi.org/10.1002/hyp.5585

Cenci, L., Laiolo, P., Gabellani, S., Campo, L., Silvestro, F., Delogu, F., Boni, G., Rudari, R., 2016. Assimilation of H-SAF Soil Moisture Products for Flash Flood Early Warning Systems. Case Study: Mediterranean Catchments. IEEE J. Sel. Top. Appl. Earth Obs. Remote Sens. PP, 5634–5646. https://doi.org/10.1109/JSTARS.2016.2598475

Chauhan, N.S., Miller, S., Ardanuy, P., 2003. Spaceborne soil moisture estimation at high resolution: a microwave-optical/IR synergistic approach. Int. J. Remote Sens. 24, 4599–4622. https://doi.org/10.1080/0143116031000156837

Cho, E., Moon, H., Choi, M., 2015. First Assessment of the Advanced Microwave Scanning Radiometer 2 (AMSR2) Soil Moisture Contents in Northeast Asia. J. Meteorol. Soc. Japan. Ser. II 93, 117–129. https://doi.org/10.2151/jmsj.2015-008

Dharssi, I., Bovis, K.J., Macpherson, B., Jones, C.P., 2011. Operational assimilation of ASCAT surface soil wetness at the Met Office. Hydrol. Earth Syst. Sci. 15, 2729–2746. https://doi.org/10.5194/hess-15-2729-2011

Dorigo, W.A., Wagner, W., Hohensinn, R., Hahn, S., Paulik, C., Xaver, A., Gruber, A., Drusch, M., Mecklenburg, S., Van Oevelen, P., Robock, A., Jackson, T., 2011. The International Soil Moisture Network: A data hosting facility for global in situ soil moisture measurements. Hydrol. Earth Syst. Sci. 15, 1675–1698. https://doi.org/10.5194/hess-15-1675-2011

Drusch, M., Wood, E.F., Gao, H., 2005. Observation operators for the direct assimilation of TRMM microwave imager retrieved soil moisture. Geophys. Res. Lett. 32, 32–35. https://doi.org/10.1029/2005GL023623

Enenkel, M., Steiner, C., Mistelbauer, T., Dorigo, W., Wagner, W., See, L., Atzberger, C., Schneider, S., Rogenhofer, E., 2016. A combined satellite-derived drought indicator to support humanitarian aid organizations. Remote Sens. 8. https://doi.org/10.3390/rs8040340

Entekhabi, D., Njoku, E.G., O'Neill, P.E., Kellogg, K.H., Crow, W.T., Edelstein, W.N., Entin, J.K., Goodman, S.D., Jackson, T.J., Johnson, J., Kimball, J., Piepmeier, J.R., Koster, R.D., Martin, N., McDonald, K.C., Moghaddam, M., Moran, S., Reichle, R., Shi, J.C., Spencer, M.W., Thurman, S.W., Tsang, L., Van Zyl, J., 2010. The soil moisture active passive (SMAP) mission. Proc. IEEE 98, 704–716. https://doi.org/10.1109/JPROC.2010.2043918

Figa-Saldaña, J., Wilson, J.J.W., Attema, E., Gelsthorpe, R., Drinkwater, M.R., Stoffelen, A., 2002. The advanced scatterometer (ASCAT) on the meteorological operational (MetOp) platform: A follow on for European wind scatterometers. Can. J. Remote Sens. 28, 404–412. https://doi.org/10.5589/m02-035

Ford, T.W., Harris, E., Quiring, S.M., 2014. Estimating root zone soil moisture using near-surface observations from SMOS. Hydrol. Earth Syst. Sci. 18, 139–154. https://doi.org/10.5194/hess-18-139-2014

Gao, X., Wu, P., Zhao, X., Zhou, X., Zhang, B., Shi, Y., Wang, J., 2013. Estimating soil moisture in gullies from adjacent upland measurements through different observation operators. J. Hydrol. 486, 420–429. https://doi.org/10.1016/j.jhydrol.2013.02.007

González-Zamora, A., Sánchez, N., Martinez-Fernandez, J., Wagner, W., 2016. Root-zone plant available water estimation using the SMOS-derived soil water index. Adv. Water Resour. 96, 339–353. https://doi.org/10.1016/j.advwatres.2016.08.001

Griesfeller, A., Lahoz, W. a., Jeu, R.A.M. d., Dorigo, W., Haugen, L.E., Svendby, T.M., Wagner, W., 2016. Evaluation of satellite soil moisture products over Norway using ground-based observations. Int. J. Appl. Earth Obs. Geoinf. 45, 155–164. https://doi.org/10.1016/j.jag.2015.04.016

Han, E., Heathman, G.C., Merwade, V., Cosh, M.H., 2012. Application of observation operators for field scale soil moisture averages and variances in agricultural landscapes. J. Hydrol. 444–445, 34–50. https://doi.org/10.1016/j.jhydrol.2012.03.035

Imaoka, K., Kachi, M., Fujii, H., Murakami, H., Hori, M., Ono, A., Igarashi, T., Nakagawa, K., Oki, T., Honda, Y., Shimoda, H., 2010. Global change observation mission (GCOM) for monitoring carbon, water cycles, and climate change. Proc. IEEE 98, 717–734. https://doi.org/10.1109/JPROC.2009.2036869

JAXA, 2013. GCOM-W1 SHIZUKU Data Users Handbook First Edition.

Kerr, Y.H., Waldteufel, P., Richaume, P., Wigneron, J.P., Ferrazzoli, P., Mahmoodi, A., Bitar, A. Al, Cabot, F., Gruhier, C., Juglea, S.E., Leroux, D., Mialon, A., Delwart, S., 2012. The SMOS Soil Moisture Retrieval Algorithm. Geosci. Remote Sens. 50, 1384–1403. https://doi.org/10.1109/TGRS.2012.2184548

Kim, K.B., Bray, M., Han, D., 2016. Exploration of optimal time steps for daily precipitation bias correction: a case study using a single grid of RCM on the River Exe in southwest England. Hydrol. Sci. J. 61, 289–301. https://doi.org/10.1080/02626667.2015.1027207

Kim, S., Liu, Y.Y., Johnson, F.M., Parinussa, R.M., Sharma, A., 2015. A global comparison of alternate AMSR2 soil moisture products: Why do they differ? Remote Sens. Environ. 161, 43–62. https://doi.org/10.1016/j.rse.2015.02.002

Koike, T., 2013. Description of GCOM-W1 AMSR2 Soil Moisture Algorithm, in: Descriptions of GCOM-W1 AMSR2 Level 1R and Level 2 Algorithms. Japan Aerospace Exploration Agency Earth Observation Research Center, p. 8.1-8.13.

Kolassa, J., Gentine, P., Prigent, C., Aires, F., 2016. Soil moisture retrieval from AMSR-E and ASCAT microwave observation synergy. Part 1: Satellite data analysis. Remote Sens. Environ. 173, 1–14. https://doi.org/10.1016/j.rse.2015.11.011

Kornelsen, K.C., Coulibaly, P., 2015. Reducing multiplicative bias of satellite soil moisture retrievals. Remote Sens. Environ. 165, 109–122. https://doi.org/10.1016/j.rse.2015.04.031

Liu, Y.Y., Parinussa, R.M., Dorigo, W.A., De Jeu, R.A.M., Wagner, W., M. Van Dijk, A.I.J., McCabe, M.F., Evans, J.P., 2011. Developing an improved soil moisture dataset by blending passive and active microwave satellite-based retrievals. Hydrol. Earth Syst. Sci. 15, 425–436. https://doi.org/10.5194/hess-15-425-2011

Lopez, A., Fung, F., New, M., Watts, G., Weston, A., Wilby, R.L., 2009. From climate model ensembles to climate change impacts and adaptation: A case study of water resource management in the southwest of England. Water Resour. Res. 45. https://doi.org/10.1029/2008WR007499

Manfreda, S., Brocca, L., Moramarco, T., Melone, F., Sheffield, J., 2014. A physically based approach for the estimation of root-zone soil moisture from surface measurements. Hydrol. Earth Syst. Sci. 18, 1199–1212. https://doi.org/10.5194/hess-18-1199-2014

Massari, C., Brocca, L., Tarpanelli, A., Moramarco, T., 2015. Data assimilation of satellite soil moisture into rainfall-runoffmodelling: A complex recipe? Remote Sens. 7, 11403–11433. https://doi.org/10.3390/rs70911403

Oliva, R., Daganzo-Eusebio, E., Kerr, Y.H., Mecklenburg, S., Nieto, S., Richaume, P., Gruhier, C., 2012. SMOS radio frequency interference scenario: Status and actions taken to improve the RFI environment in the 1400-1427-MHZ passive band. IEEE Trans. Geosci. Remote Sens. 50, 1427–1439. https://doi.org/10.1109/TGRS.2012.2182775

Owe, M., de Jeu, R., Holmes, T., 2008. Multisensor historical climatology of satellite-derived global land surface moisture. J. Geophys. Res. Earth Surf. 113, 1–17.

https://doi.org/10.1029/2007JF000769

Paquette, M., Fortier, D., Vincent, W., 2016. Water tracks in the High Arctic: A hydrological network dominated by rapid subsurface flow through patterned ground Journal: Arct. Sci. 353, 334–353.

Paulik, C., Dorigo, W., Wagner, W., Kidd, R., 2014. Validation of the ASCAT soil water index using in situ data from the International Soil moisture network. Int. J. Appl. Earth Obs. Geoinf. 30, 1–8. https://doi.org/10.1016/j.jag.2014.01.007

Peng, J., Loew, A., Merlin, O., Verhoest, N.E.C., 2017. A review of spatial downscaling of satellite remotely sensed soil moisture. Rev. Geophys. 1–26. https://doi.org/10.1002/2016RG000543

Qiu, J., Crow, W.T., Nearing, G.S., Mo, X., Liu, S., 2014. The impact of vertical measurement depth on the information content of soil moisture times series data. Geophys. Res. Lett. 41, 4997–5004. https://doi.org/10.1002/2014GL060017

Reichle, R.H., KOSTER, R.D., Dong, J., Berg, A.A., 2004. Global Soil Moisture from Satellite Observations , Land Surface Models , and Ground Data : Implications for Data Assimilation. J. Hydrometeorol. 5, 430–443.

Renzullo, L.J., van Dijk, A.I.J.M., Perraud, J.M., Collins, D., Henderson, B., Jin, H., Smith, A.B., McJannet, D.L., 2014. Continental satellite soil moisture data assimilation improves root-zone moisture analysis for water resources assessment. J. Hydrol. 519, 2747–2762. https://doi.org/10.1016/j.jhydrol.2014.08.008

Sabater, J.M., Jarlan, L., Calvet, J.-C., Bouyssel, F., De Rosnay, P., 2007. From Near-Surface to Root-Zone Soil Moisture Using Different Assimilation Techniques. J. Hydrometeorol. 8, 194–206. https://doi.org/10.1175/JHM571.1

Scipal, K., Drusch, M., Wagner, W., 2008. Assimilation of a ERS scatterometer derived soil moisture index in the ECMWF numerical weather prediction system. Adv. Water Resour. 31, 1101–1112. https://doi.org/10.1016/j.advwatres.2008.04.013

Su, C.H., Ryu, D., Young, R.I., Western, A.W., Wagner, W., 2013. Inter-comparison of microwave satellite soil moisture retrievals over the Murrumbidgee Basin, southeast Australia. Remote Sens. Environ. 134, 1–11. https://doi.org/10.1016/j.rse.2013.02.016

Wagner, W., Hahn, S., Kidd, R., Melzer, T., Bartalis, Z., Hasenauer, S., Figa-Saldaña, J., De Rosnay, P., Jann, A., Schneider, S., Komma, J., Kubu, G., Brugger, K., Aubrecht, C., Züger, J., Gangkofner, U., Kienberger, S., Brocca, L., Wang, Y., Blöschl, G., Eitzinger, J., Steinnocher, K., Zeil, P., Rubel, F., 2013. The ASCAT soil moisture product: A review of its specifications, validation results, and emerging applications. Meteorol. Zeitschrift 22, 5–33. https://doi.org/10.1127/0941-2948/2013/0399

Wagner, W., Lemoine, G., Rott, H., 1999. A method for estimating soil moisture from ERS Scatterometer and soil data. Remote Sens. Environ. 70, 191–207. https://doi.org/10.1016/S0034-4257(99)00036-X

Wu, Q., Liu, H., Wang, L., Deng, C., 2016. Evaluation of AMSR2 soil moisture products over the contiguous United States using in situ data from the International Soil Moisture Network. Int. J. Appl. Earth Obs. Geoinf. 45, 187–199. https://doi.org/10.1016/j.jag.2015.10.011

Yang, W., Andréasson, J., Phil Graham, L., Olsson, J., Rosberg, J., Wetterhall, F., 2010. Distribution-based scaling to improve usability of regional climate model projections for hydrological climate change impacts studies. Hydrol. Res. 41, 211. https://doi.org/10.2166/nh.2010.004

Zaman, B., Mckee, M., 2014. Spatio-Temporal Prediction of Root Zone Soil Moisture Using Multivariate Relevance Vector Machines. Open J. Mod. Hydrol. 4, 80–90. https://doi.org/dx.doi.org/10.4236/ojmh.2014.43007

Zeng, J., Li, Z., Chen, Q., Bi, H., Qiu, J., Zou, P., 2015. Evaluation of remotely sensed and reanalysis soil moisture products over the Tibetan Plateau using in-situ observations. Remote Sens. Environ. 163, 91–110. https://doi.org/10.1016/j.rse.2015.03.008

Zhuo, L., Han, D., 2016. Could operational hydrological models be made compatible with satellite soil moisture observations? Hydrol. Process. 30, 1637–1648. https://doi.org/10.1002/hyp.10804

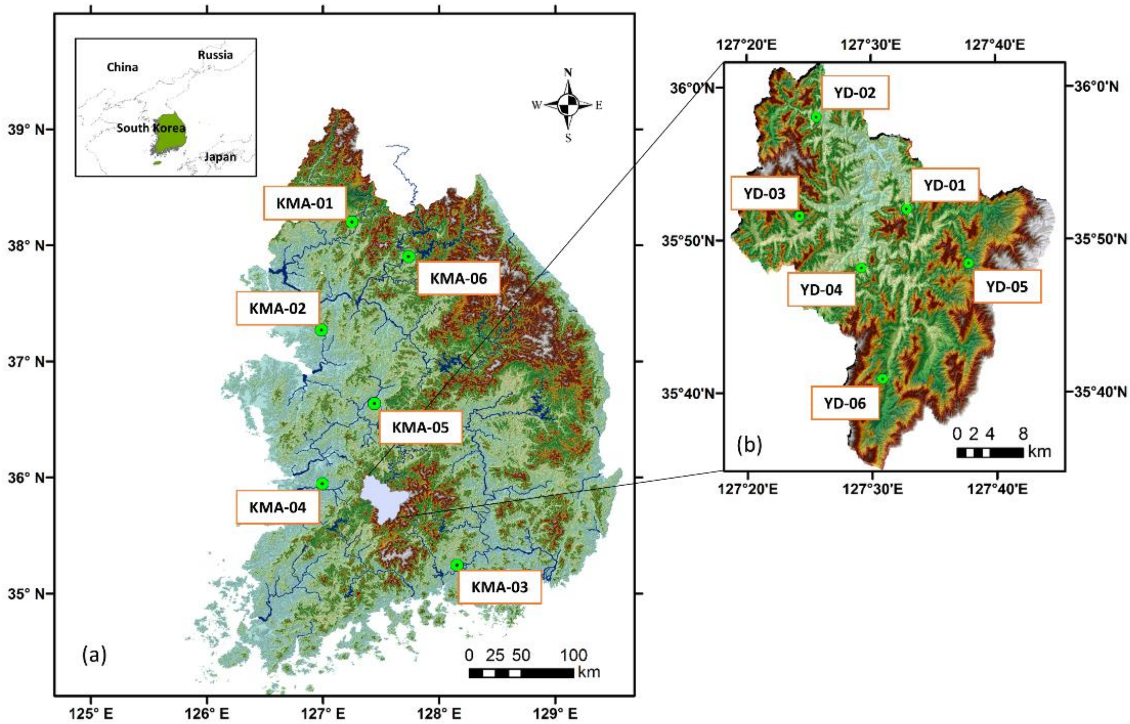

Figure 1. Locations of the two networks. The base map shows the elevation of the corresponding area. KMA and YD represent (a) Korea meteorological Administration networks, and (b) Korea Water Resources Cooperation networks, respectively.

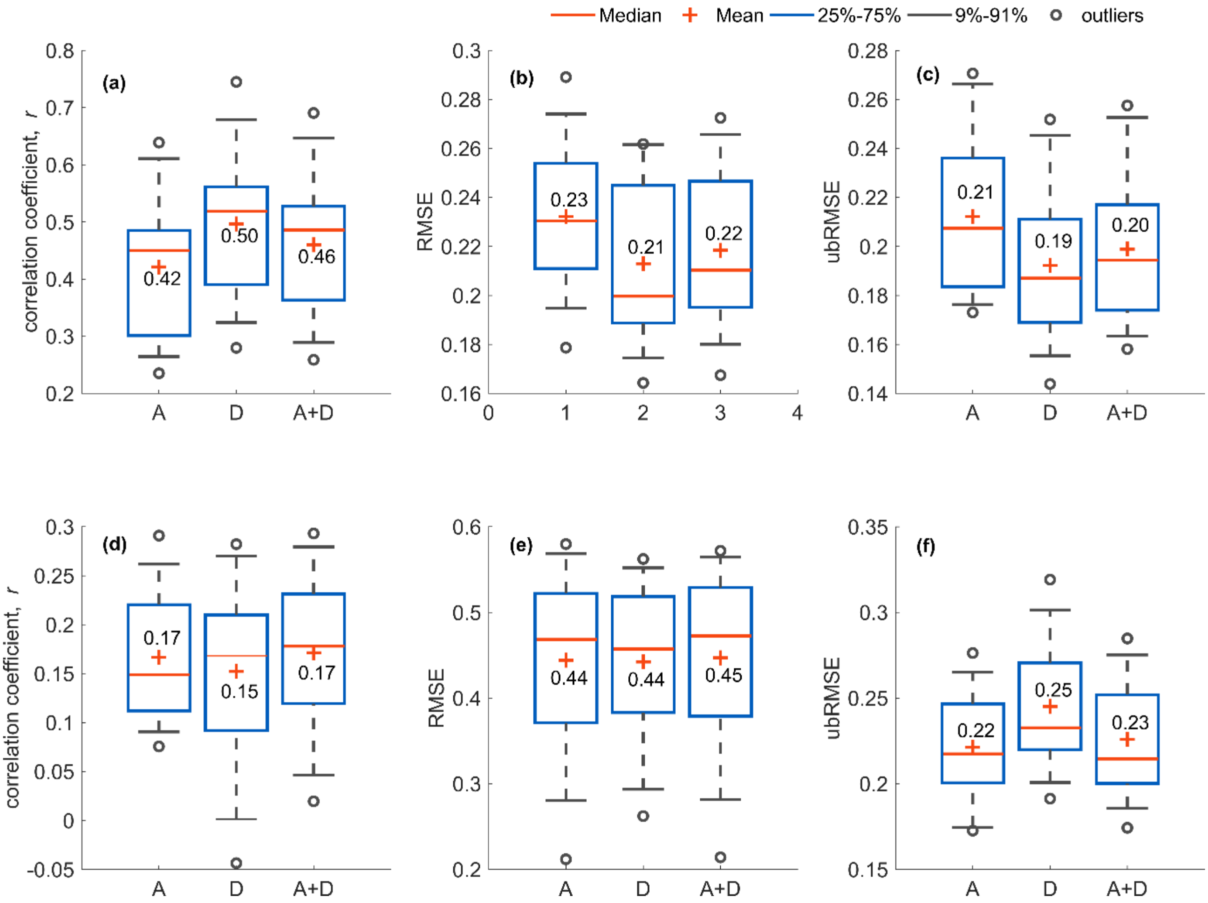

Figure 2. Boxplots of correlation coefficient (r), RMSE and ubRMSE: (a-c) for ASCAT and (d-f) for AMSR2. Here, the x-axis indicates satellite orbits; (A) and (D) correspond to the ascending and descending overpasses, respectively. (A+D) refers to the aggregation of the ascending and descending overpasses.

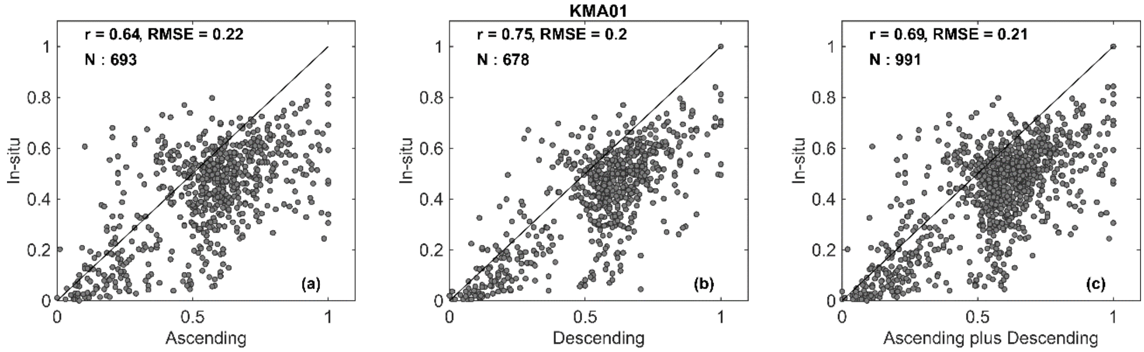

Figure 3. Statistical scores (*r* and RMSE) between ASCAT SM and site-specific data sets for the KMA01 site. N indicates the number of data pairs.

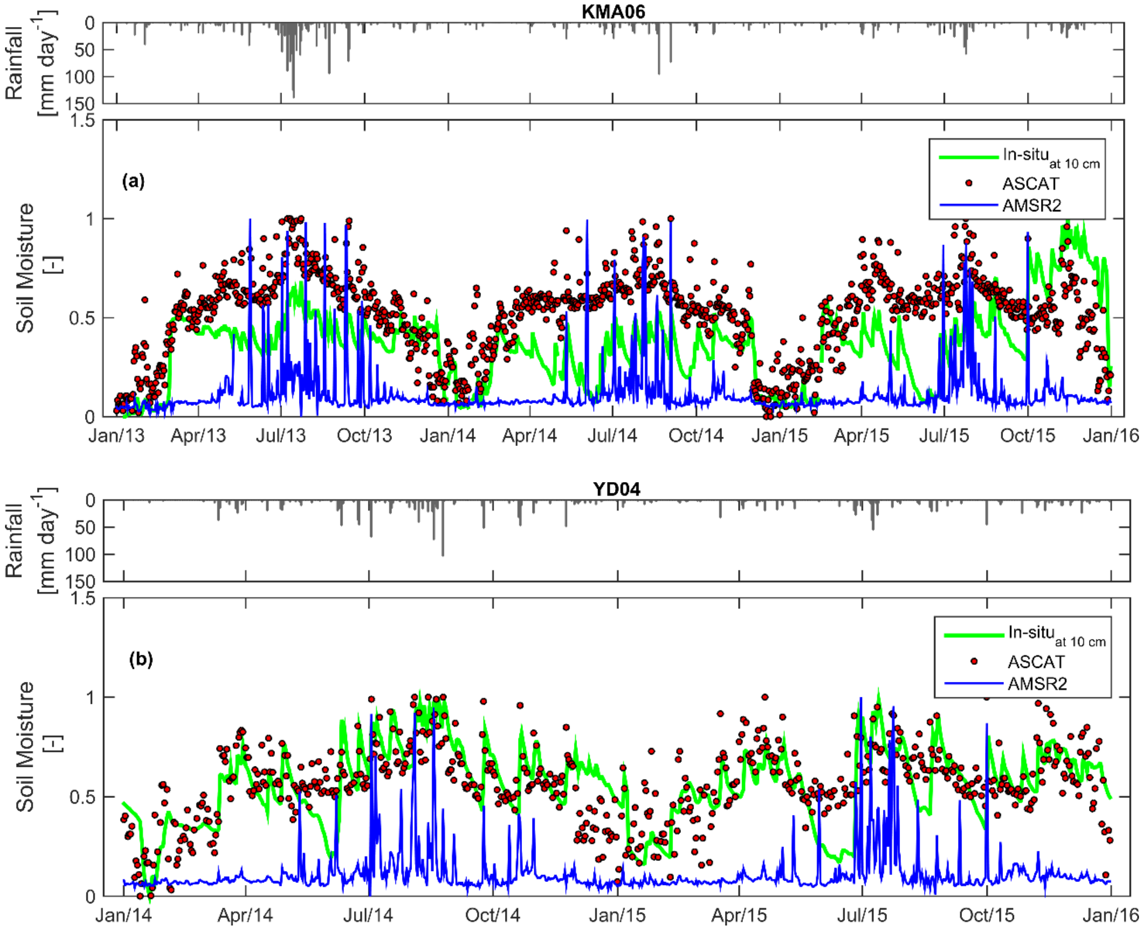

Figure 4. Samples of time series comparison of SM products (ASCAT and AMSR2) with in-situ observations. The bar graph indicates rainfall.

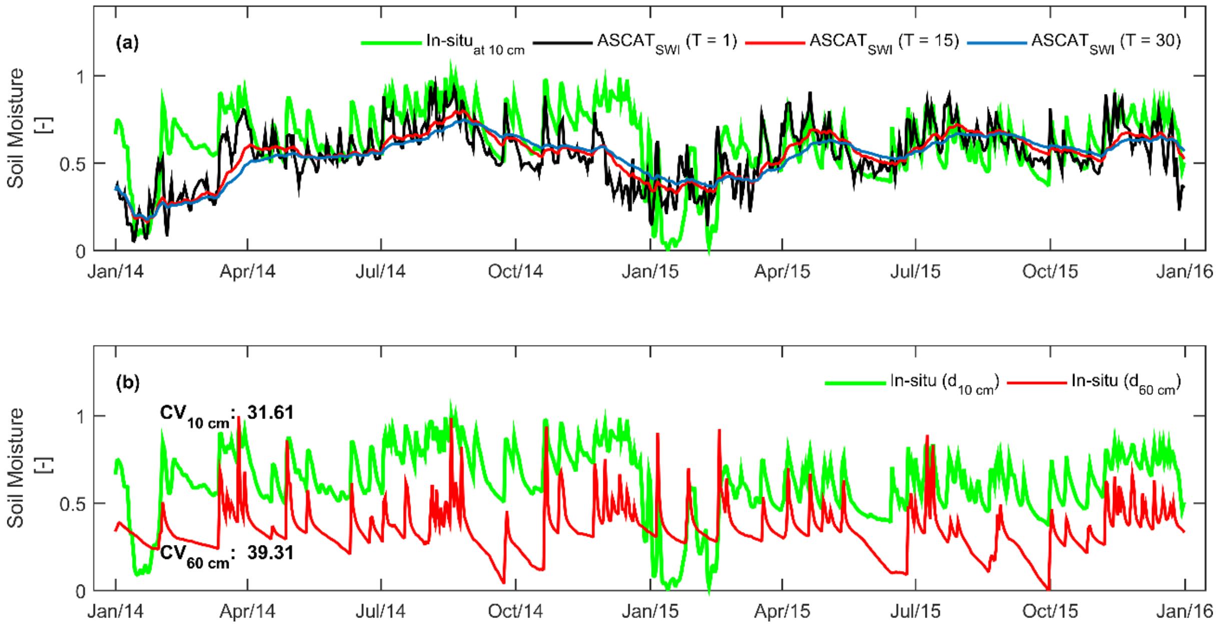

Figure 5. (a) In-situ SM measurements and ASCAT SWI time series from the YD03 site with different *T* (1, 15 and 30 days). (b) in-situ observations at different observation depths along with coefficient of variation (CV).

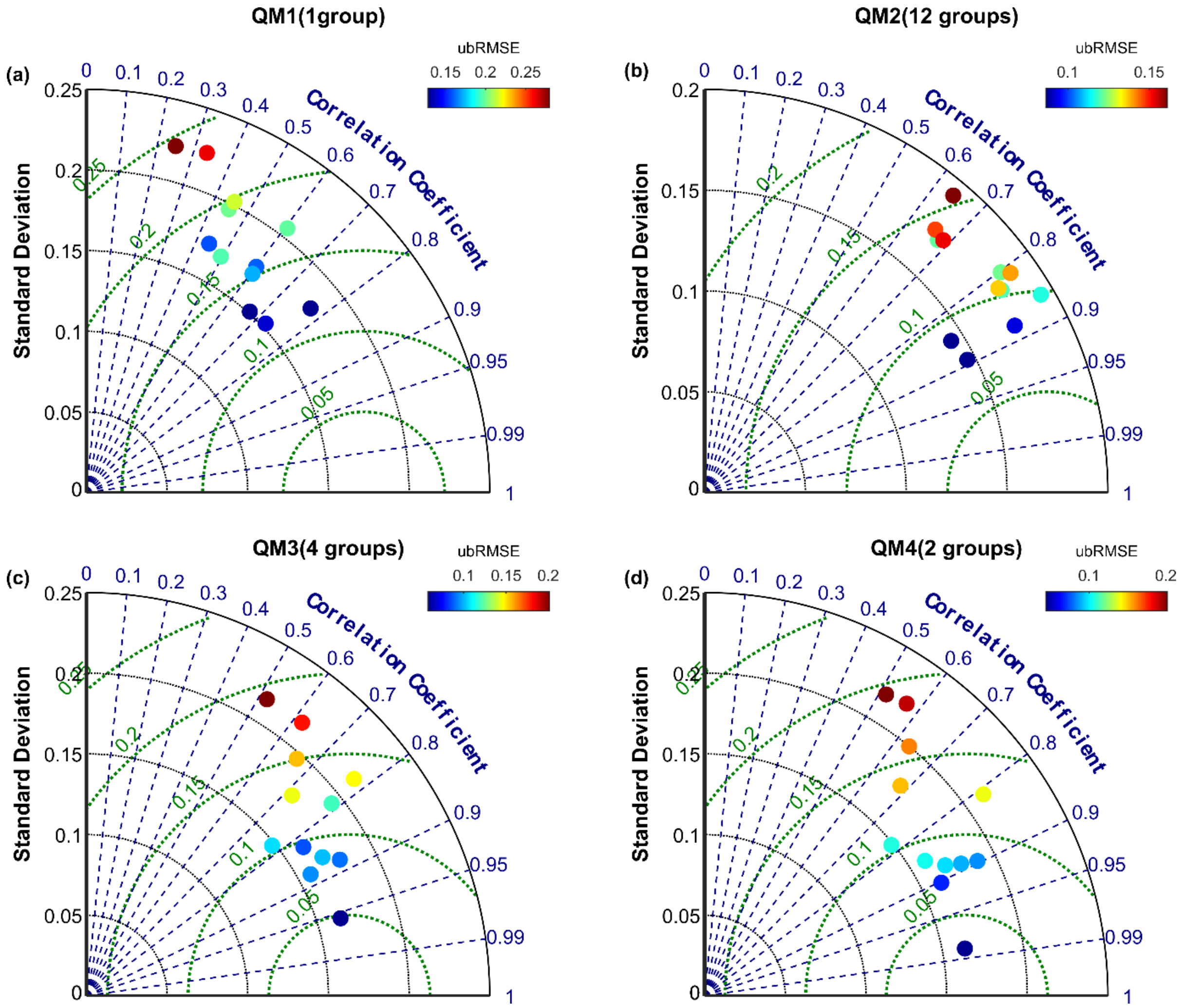

Figure 6. Taylor diagram representing the statistics between the in-situ observations measured at 10 cm depth and ASCAT SWI-CDF at 12 sites.

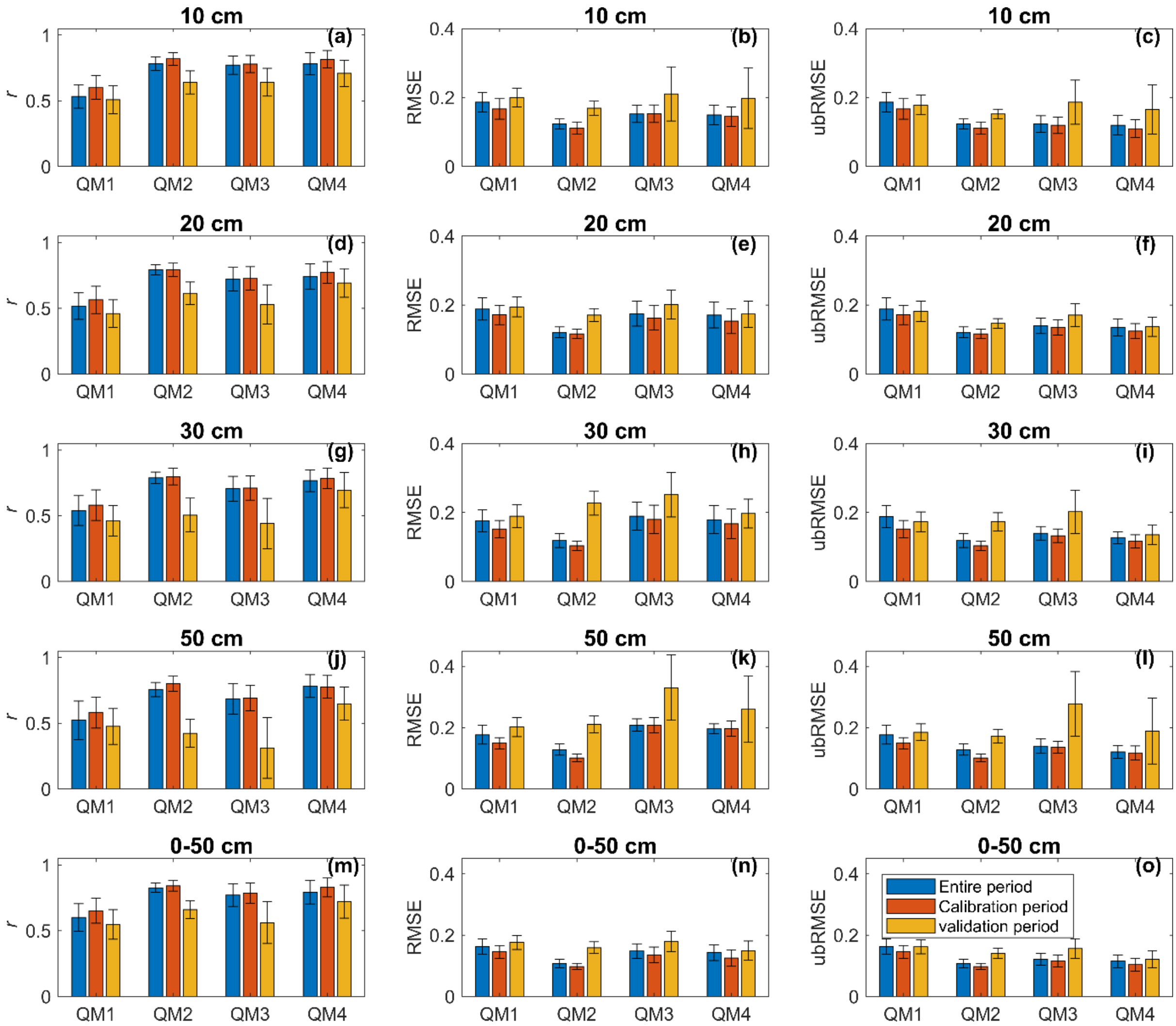

Figure 7. Statistics of the correlation coefficient (*r*), RMSE, and ubRMSE. Here, the error bar indicates 95% confidence interval.

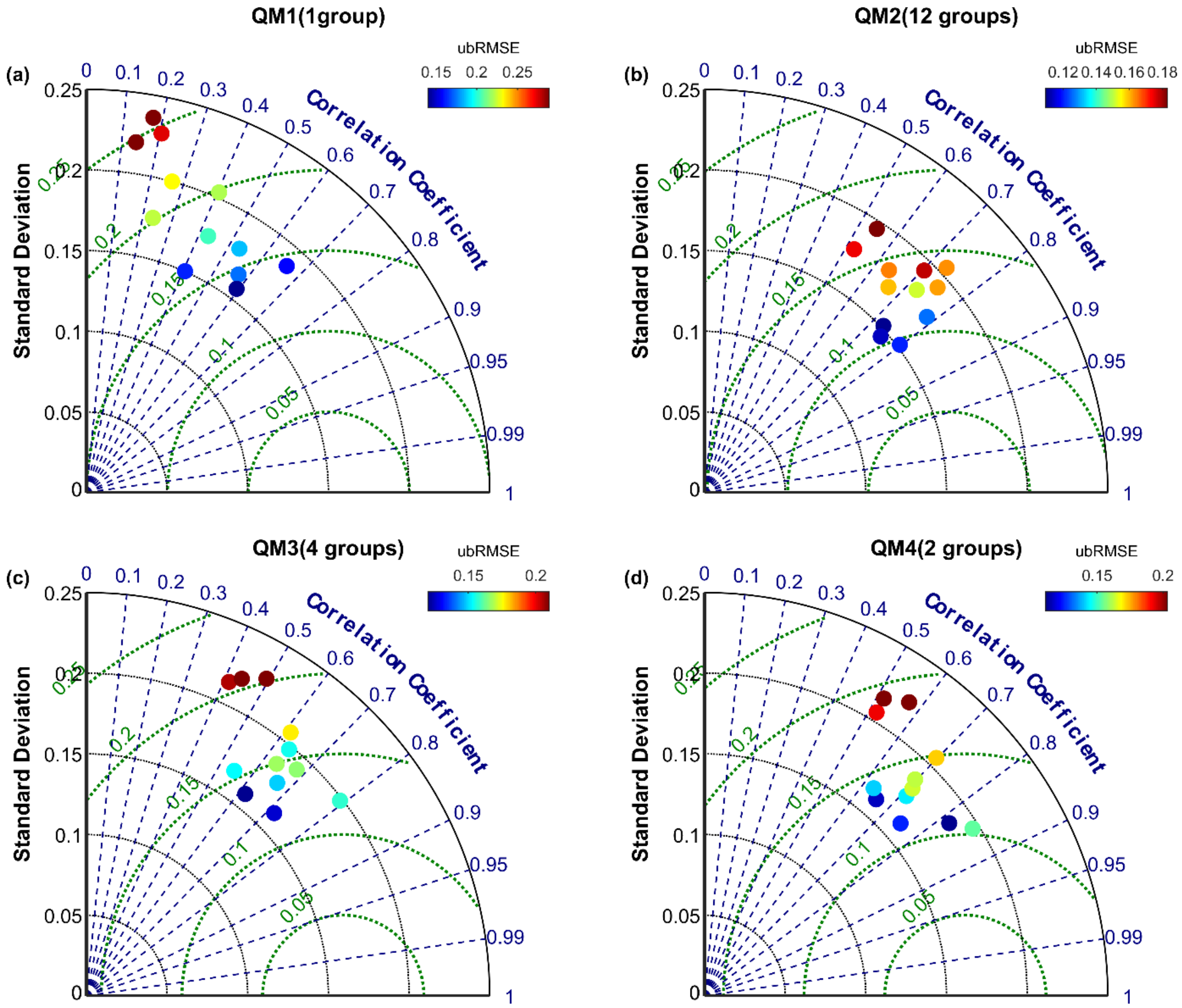

Figure 8. Taylor diagram representing the statistics between the in-situ observations measured at 10 cm depth and AMSR2 SWI-CDF at 12 sites.

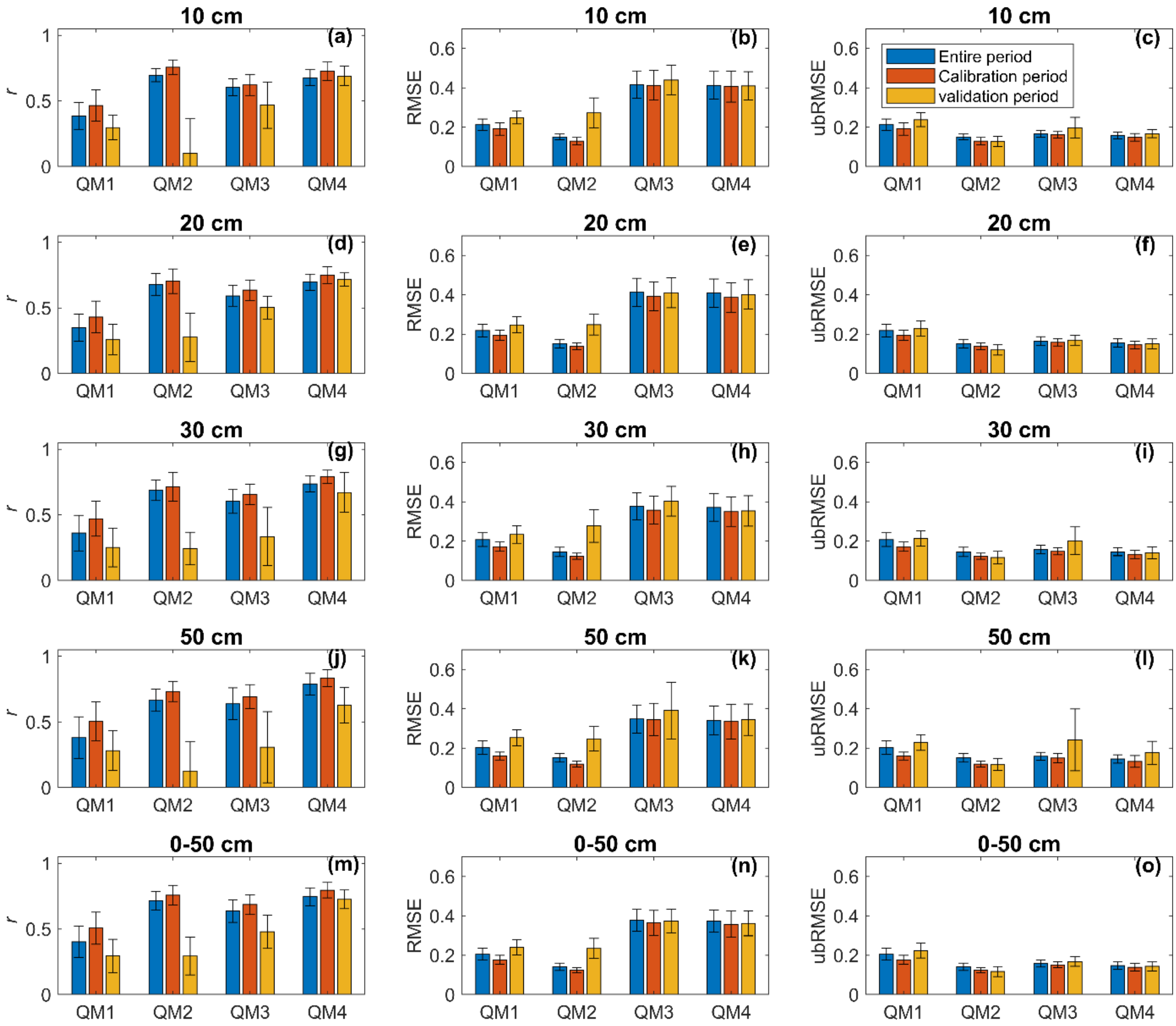

Figure 9. Statistics of the correlation coefficient (r), and RMSE. Here, the error bar indicates 95% confidence interval.

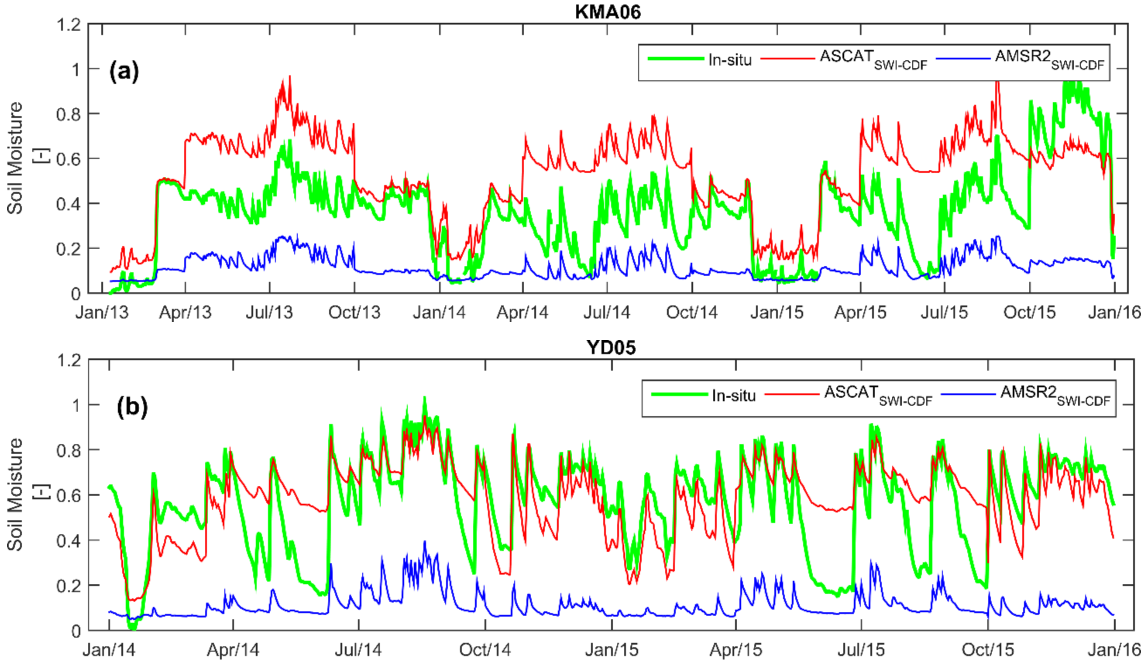

Figure 10. Time series of in-situ observation measured at 10 cm depth and SWI-CDF products. Here, the results of the QM4 group are presented.

Table 1. Main characteristics of the study sites. Here, water fraction indicates the area ratio of wetlands plus open water surfaces within ASCAT pixel (12.5 km).

Site	Elevation (m a.s.l)	Longitude (º)	Latitude (º)	Annual rainfall (mm/year)	Observation depth (cm)	Land use	Water ratio (%)	Period
KMA-01	181.0	127.25	38.20	1,179	10, 20, 30, 50	Forest	1.6	2013-2015
KMA-02	33.6	126.99	37.27	1,007	10, 20, 30, 50	Agriculture	3.2	2013-2015
KMA-03	22.0	128.15	35.24	1,397	10, 20, 30, 50	Forest	4.5	2013-2015
KMA-04	15.0	126.99	35.95	1,095	10, 20, 30, 50	Agriculture	3.9	2013-2015
KMA-05	56.4	127.44	36.63	970	10, 20, 30, 50	Agriculture	2.2	2013-2015
KMA-06	76.8	127.74	37.9	1,058	10, 20, 30, 50	Forest	9.1	2013-2015
YD-01	313.0	127.55	35.87	1,011	10, 20, 40, 60, 80	Forest	2.0	2014-2015
YD-02	330.0	127.43	35.97	1,111	10, 20, 40, 60	Forest	0.7	2014-2015
YD-03	396.0	127.40	35.86	1,108	10, 20, 40, 60	Forest	0.4	2014-2015
YD-04	334.0	127.49	35.80	1,043	10, 20, 40, 60, 80	Forest	1.4	2014-2015
YD-05	453	127.63	35.81	956	10, 20, 40, 60, 80	Forest	0.6	2014-2015
YD-06	409.0	127.51	35.68	1,071	10, 20, 40, 60, 80	Forest	0.7	2014-2015

Table 2. Comparison of different retrieval algorithms for AMSR2 SM products.

Algorithm	**Frequency**	**mean *r***	**mean RMSE**	**mean Bias**	**max *r***	**Min *r***
JAXA	10.7	0.17	0.45	0.38	0.29	0.02
LPRM (X)	10.7	0.13	0.29	0.00	0.40	-0.20
(C1)	6.9	0.15	0.33	-0.20	0.27	0.04
(C2)	7.3	0.17	0.32	-0.08	0.26	0.02

Table 3. Comparison of ASCAT SWI with different observation depths (r: correlation coefficient, RMSE: root mean square error, T: characteristic time length (days)).

Site	**D_{10cm}**				**$D_{20\,cm}$**				**$D_{30\,cm}$**				**$D_{50\,cm}$**				**$D_{0\text{-}50\,cm}$**			
	r	**RMSE**	**ubRMSE**	***T***	***r***	**RMSE**	**ubRMSE**	***T***	***r***	**RMSE**	**ubRMSE**	***T***	***r***	**RMSE**	**ubRMSE**	***T***	***r***	**RMSE**	**ubRMSE**	***T***
KMA01	0.74	0.19	0.15	2.1	0.69	0.33	0.14	2.5	0.73	0.38	0.13	4.7	0.71	0.23	0.15	16.7	0.83	0.24	0.11	2.5
KMA02	0.42	0.22	0.15	1.7	0.70	0.13	0.12	4.1	0.67	0.15	0.14	4.3	0.66	0.20	0.16	3.9	0.71	0.14	0.13	2.9
KMA03	0.44	0.19	0.19	1.7	0.47	0.17	0.17	2.7	0.46	0.21	0.18	4.7	0.63	0.22	0.14	4.5	0.62	0.15	0.14	2.1
KMA04	0.59	0.16	0.15	2.3	0.63	0.24	0.18	5.9	0.60	0.22	0.18	6.9	0.39	0.29	0.19	6.3	0.63	0.17	0.17	3.1
KMA05	0.63	0.18	0.17	2.9	0.65	0.14	0.15	5.7	0.68	0.16	0.12	19.9	0.66	0.23	0.11	19.9	0.70	0.13	0.14	4.1
KMA06	0.53	0.25	0.18	4.3	0.61	0.18	0.18	11.3	0.51	0.21	0.14	19.9	0.21	0.43	0.14	19.9	0.53	0.26	0.15	8.1
YD01	0.65	0.16	0.13	4.3	0.53	0.23	0.17	3.3	0.45	0.29	0.20	2.9	0.74	0.22	0.17	5.9	0.59	0.20	0.16	2.9
YD02	0.31	0.25	0.24	2.3	0.22	0.26	0.24	2.1	0.25	0.23	0.22	1.7	0.06	0.23	0.22	1.3	0.28	0.22	0.22	1.3
YD03	0.60	0.18	0.16	3.7	0.47	0.19	0.17	2.5	0.39	0.20	0.20	3.1	0.29	0.27	0.17	1.5	0.55	0.17	0.16	2.1
YD04	0.76	0.12	0.14	5.5	0.66	0.15	0.15	6.7	0.76	0.18	0.14	8.9	0.68	0.21	0.15	9.3	0.76	0.16	0.15	6.5
YD05	0.46	0.20	0.20	3.3	0.30	0.23	0.22	3.7	0.17	0.24	0.24	4.9	0.12	0.27	0.27	5.5	0.34	0.22	0.20	3.3
YD06	0.39	0.22	0.22	3.1	0.32	0.23	0.23	3.3	0.42	0.21	0.18	4.7	0.44	0.24	0.20	5.3	0.41	0.21	0.20	3.1
Average	0.54	0.19	0.17	3.1	0.52	0.21	0.18	4.5	0.51	0.22	0.17	7.2	0.47	0.25	0.17	8.3	0.58	0.19	0.16	3.5

Table 4. Comparison of AMSR2 SWI with different observation depths (r: correlation coefficient, RMSE: root mean square error, *T*: characteristic time length (days)).

Site	D $_{10cm}$				D $_{20cm}$				D $_{30cm}$				D $_{50cm}$				D $_{0\text{-}50\ cm}$			
	r	RMSE	ubRMSE	*T*	r	RMSE	ubRMSE	*T*	r	RMSE	ubRMSE	*T*	r	RMSE	ubRMSE	*T*	r	RMSE	ubRMSE	*T*
KMA01	0.49	0.32	0.17	7.3	0.51	0.16	0.11	7.1	0.64	0.10	0.08	19.1	0.72	0.28	0.16	17.7	0.70	0.18	0.10	13.9
KMA02	0.39	0.17	0.14	29.9	0.46	0.26	0.15	5.3	0.46	0.35	0.16	5.1	0.46	0.23	0.19	4.3	0.49	0.26	0.16	5.1
KMA03	0.29	0.37	0.21	2.7	0.11	0.37	0.23	2.5	0.00	0.31	0.25	2.3	0.19	0.24	0.21	3.5	0.18	0.32	0.21	2.7
KMA04	0.16	0.41	0.20	2.7	0.14	0.51	0.24	5.5	0.14	0.48	0.24	6.1	0.18	0.56	0.21	7.9	0.16	0.42	0.24	3.9
KMA05	0.10	0.44	0.24	2.7	0.17	0.47	0.19	29.9	0.25	0.52	0.16	29.9	0.44	0.24	0.14	29.9	0.21	0.43	0.18	29.9
KMA06	0.40	0.31	0.18	29.9	0.46	0.45	0.21	29.9	0.61	0.43	0.15	28.3	0.69	0.50	0.16	29.9	0.59	0.41	0.17	28.9
YD01	0.54	0.55	0.14	7.7	0.50	0.33	0.16	6.3	0.38	0.32	0.20	5.5	0.61	0.38	0.22	21.7	0.49	0.38	0.17	6.7
YD02	0.23	0.56	0.23	3.1	0.19	0.55	0.23	3.1	0.18	0.45	0.20	2.7	0.07	0.49	0.17	3.5	0.20	0.53	0.21	3.1
YD03	0.42	0.53	0.18	11.5	0.34	0.53	0.17	4.3	0.36	0.49	0.19	5.9	0.29	0.27	0.14	3.1	0.40	0.42	0.17	5.1
YD04	0.62	0.47	0.17	18.9	0.58	0.48	0.17	23.1	0.71	0.38	0.18	29.9	0.63	0.34	0.17	25.7	0.66	0.41	0.18	25.7
YD05	0.41	0.49	0.19	6.5	0.26	0.48	0.21	7.3	0.20	0.48	0.20	12.7	0.15	0.47	0.24	12.3	0.31	0.45	0.19	9.3
YD06	0.25	0.50	0.23	4.1	0.17	0.51	0.23	4.3	0.22	0.37	0.17	8.1	0.20	0.36	0.20	10.5	0.22	0.45	0.20	5.3
Average	0.36	0.43	0.19	10.6	0.33	0.42	0.19	10.7	0.34	0.39	0.18	13.0	0.39	0.36	0.18	14.2	0.38	0.39	0.18	11.6